# SAR500 - A High-Precision High-Stability Butterfly Gyroscope with North Seeking Capability

Daniel Lapadatu, Bjørn Blixhavn, Reidar Holm and Terje Kvisterøy
Sensonor Technologies AS
Horten, Norway
daniel.lapadatu@sensonor.no

*Abstract*— **This paper describes a novel high-precision, low-noise, high-stability, calibrated and compensated digital oscillatory gyroscope with SPI interface, housed in custom-made ceramic packages. The device is factory-calibrated and compensated for temperature effects to provide high-accuracy digital output over a broad temperature range. Optimized tuning of the excitation and detection frequencies, as well as optimized mechanical and electrical balancing result in low sensitivity to shock and vibrations. By utilizing a unique sealed cavity technology, the vibrating elements of the gyroscope are contained within the low-pressure hermetic environment needed for high Q factors. Further on, improved stability of the device is achieved by full design symmetry, high thermal efficiency and choice of crystalline materials in the entire structure.**

***Keywords: low-noise, high-stability, high-performance, north seeking capable MEMS gyroscope.***

## I. INTRODUCTION

There is an ever increasing need for high-precision, high-stability, miniaturized and batch-manufactured MEMS angular rate sensors for inertial navigation, positioning, stabilization, tracking and guidance of remote operated devices [1]. In the market of tactical and inertial grade MEMS gyroscopes, proving the reliability and long-term stability of these devices remains probably the greatest challenge.

SAR500, a robust tuning fork type MEMS gyroscope with SPI communication, has been designed for vibration-exposed applications operating in harsh environments. It is based on the well proven Sensonor ButterflyGyro™ structure [2].

For operating as angular rate sensors, the tuning fork type gyroscopes require arrangements with at least two orthogonal degrees of freedom. In such devices, a certain known primary motion, corresponding to the first degree of freedom, must be generated and maintained in the sensor. An external angular velocity affecting the sensor in a direction perpendicular to the primary motion induces an oscillating Coriolis force in a direction corresponding to the second degree of freedom. The induced Coriolis force is proportional with the external angular velocity and the amplitude of the primary motion. It is therefore necessary to generate, maintain and control a primary oscillation with large amplitude, achievable only by structures sealed in high vacuum, exhibiting high quality factors [3, 4].

Commonly, in silicon-based tuning fork gyroscopes, the primary motion is initiated and maintained at right angles to the substrate surface by means of electrostatic excitation. However, the rather low oscillation amplitude will cause these types of gyroscopes to suffer from lower gyroscopic scale factors.

This problem has been addressed by using beams that have a tendency to bend in a direction that is substantially parallel to the plane of the substrate, such as the asymmetric beams reported in [2] and [5], thus allowing primary motions with large oscillation amplitudes.

A limitation in many existing devices is the presence of non-uniform characteristics and built-in stress that can cause unintended sensitivity to external mechanical and thermal loads or unpredictable drift of characteristics. This problem has been previously addressed mainly by use of stress-release structures and pedestals [6-8]. In order to further improve the uniformity of the mechanical characteristics and the long-term stability of the gyroscope, a new fabrication method has been developed [9]. This method allows the use of single-crystal silicon in the entire structure of the device, including the capping wafers, while enabling the hermetic sealing of the vibrating elements by means of anodic bonding.

Closed feed-back loops are used to control the excitation and detection modes. Furthermore, SAR500 uses additional electrodes in order to continuously adjust the frequency of the oscillations and actively compensate the quadrature bias.

Particular to the design of SAR500 gyroscope is the full horizontal and vertical symmetry of the device at all levels, as well as the double-side excitation, detection, adjustment and compensation arrangements.

The SAR500 contains a ButterflyGyro™ MEMS die and an analog ASIC, individually housed in rigid, fully symmetrical, custom-made ceramic packages with high thermal efficiency, which further improves the device long-term stability. An additional digital ASIC, or an FPGA, contains the needed control and functional algorithms to achieve the superior performance.

This work has been sponsored by:
Research Council of Norway, "SIMU", Contract No. 193254/I40, and
European Commission, "SIMU-SiP", Eurostars, Contract No. E! 4736.

## II. SENSOR DESIGN AND OPERATION

### A. Operation principle

The sensing element, manufactured entirely in a single-crystal silicon substrate, consists of two identical seismic masses suspended by means of asymmetric driving beams to pedestals designed to minimize the mechanical and thermal stress. The two masses are connected to each other by means of a centrally located synchronizing beam.

The seismic masses and the beams are arranged to provide a first degree of rotational freedom about the excitation axes, which are perpendicular to the plane of the substrate, and a second degree of rotational freedom about the detection axis, which is coincident with the longitudinal axis of the beams, as illustrated in Fig. 1.

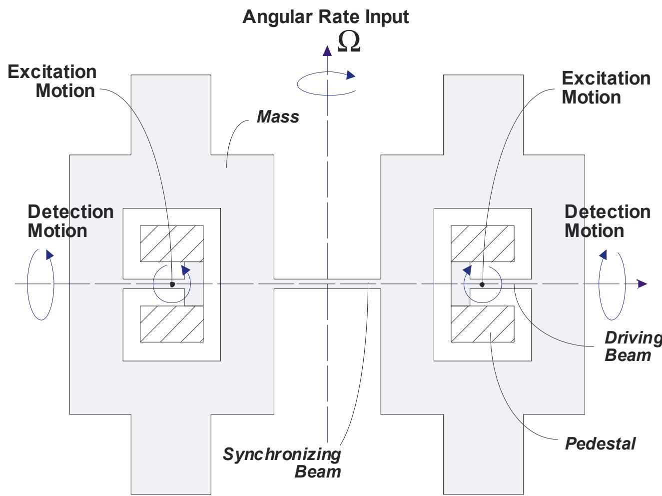


Figure 1. Excitation and detection motions in the ButterflyGyro™.

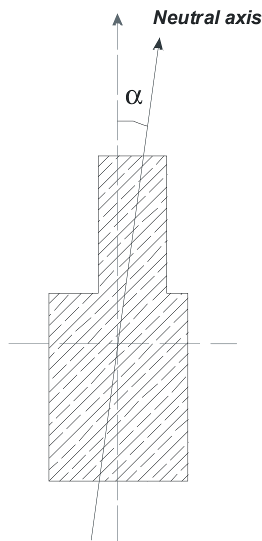


Figure 2. Cross-sectional view of the asymmetric beam.

The beams, all having identical cross-sectional geometry, exhibit an asymmetric cross-section, as illustrated in Fig. 2. The neutral axis of the beams forms an acute, non-zero angle α with the normal excitation axes. The beams have thus the tendency to bend in a direction that is mostly parallel to the plane of the substrate, so that an in-plane oscillation of the masses may be initiated by a force that is perpendicular to the plane of the substrate [2].

The driving beams are dimensioned in such a way that the resonance frequency of the in-plane bending mode matches the resonance frequency of the torsion mode. Henceforward, the in-plane bending mode of the springs will be referred as "primary" or "excitation" mode, while the torsion mode will be referred as "secondary" or "detection" mode.

When excitation is applied the masses vibrate in opposing phases and parallel to the plane of the substrate, which results in large gyroscopic moments in the presence of angular rate inputs along an axis located in the plane of the substrate and perpendicular to the beams.

Capacitive schemes, operating in closed feedback loops, are employed to initiate, control and accurately quantify the primary and secondary motions.

The vibrating structure, formed by the two seismic masses and the beams, is attached to and hermetically sealed between two, fully symmetrical capping silicon-glass composite wafers [10, 11], as illustrated in Fig. 3. A silicon frame, manufactured in the same single-crystal silicon substrate, surrounds the vibrating structure. The frame and pedestals are attached to the silicon-glass composite wafers by means of anodic bonding in high vacuum. The vibrating masses are thus contained within the low-pressure hermetic environment needed for high Q factors.

The composite wafers contain fully symmetrical patterns of silicon and glass inserts. The silicon patterns form fixed electrodes electrically isolated from each other by narrow glass inserts. Additionally, some wider glass inserts serve as attachment surfaces between the silicon substrate and the composite wafers during the anodic bonding.

Recesses are symmetrically etched on both sides of the silicon substrate to form the gaps of the capacitors.

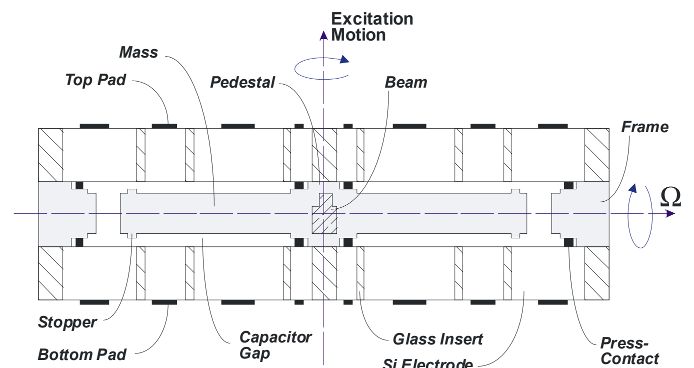


Figure 3. Cross-sectional view of the sensing element.

The fixed electrodes are either actively used during the operation of the device or configured as screening electrodes, the latter being electrically connected to the masses and the frame by means of metallic press-contacts accommodated in dedicated recesses. Silicon stoppers, in combination with the screening electrodes, are employed to prevent stiction and electrical short-circuiting between the moving masses and the active electrodes.

Pads for external electrical connection are provided on the outer surfaces of the capping wafers.

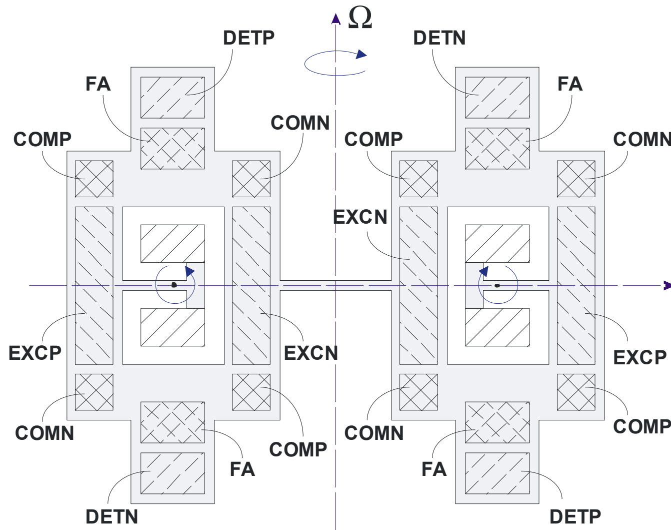


Figure 4. Top side configuration of the active electrodes.

The top side configuration of the active electrodes is shown in Fig. 4. Except for the polarity of the electrodes, an identical configuration is valid for the bottom side of the device. Pairs of identical electrodes, located above and below each seismic mass, are symmetrically disposed with respect to the excitation and detection axes.

Four pairs of "excitation" electrodes, designated as "EXCP" and "EXCN", are used to initiate, detect and control the primary motion of the masses.

Four pairs of "detection" electrodes, designated as "DETP" and "DETN", are used to detect and control the secondary motion of the masses. The amplitude of the secondary oscillations is directly proportional to the external angular velocity Ω and the amplitude of the primary oscillations.

Four pairs of "adjustment" electrodes, designated as "FA", are used to continuously adjust and fine-tune the resonance frequency of the primary and secondary oscillations.

Eight pairs of "compensation" electrodes, designated as "COMP" and "COMN", are used to actively compensate the quadrature bias.

The frequency matching and the quadrature compensation are achieved by applying tunable, DC voltages between the seismic masses and the respective electrodes, in combination with innovative algorithms implemented in the associated electronic circuits. Further reduction of the quadrature bias is achieved by minimizing the capacitive coupling between the excitation and detection loops.

### *B. Low-Noise, High-Stability Design*

The design targets for the noise level and stability of the sensor element were roughly half of those available for the entire device, with the other half being allocated to the ASICs.

In some particular instances, such as the size of the masses or the thickness of the glass inserts, a trade-off between the low-noise and high-stability requirements had to be resolved.

In general for capacitive MEMS gyroscopes, the only major source of noise in the sensing element is the mechanical (Brownian) noise associated with the various damping mechanisms, such as gas damping and thermoelastic damping.

The gas damping is minimized by hermetically sealing the vibrating structure in high-vacuum. The thermoelastic damping is minimized by optimal design of the spring geometry [12].

Regardless of the damping mechanism, larger masses, lower spring constants and reduced electrode gaps help to decrease even further the Brownian noise floor.

For capacitive MEMS gyroscopes in general, the main sources of drift and instability in the sensing element are: non-uniform thermal and mechanical loads, variation of the residual gas pressure and humidity, creep and hysteresis of materials, fatigue in the vibrating beams, and the electrostatic charging of dielectrics.

The use of high quality, defect free, single-crystal silicon in the entire structure of the sensing element, including the two capping wafers, substantially reduces the thermally-generated stress, the creep and the risk of fatigue. To reduce even further the risk of fatigue, the driving beams are dimensioned in such a way that the cyclic load stress is kept at rather low values.

To minimize the package-related mechanical and thermal stress level, the vibrating structures are anchored by means of pedestals and stress-release springs. An innovative mounting technique in a vacuum ceramic package further decouples the sensing element from the environment.

The slow, yet irreversible, drift in the gas pressure, caused by temperature-induced outgassing, is kept under control by using a suitable getter material.

Within the operating range of temperatures, water is probably the only material found in the environment that can exists in all states of aggregation. Water changing between solid, liquid and vapour phases is therefore a major source of instability. Special care has been taken to reduce the amount of water present during the bonding of the wafers.

Parasitic charging of dielectric surfaces is another major factor that limits the stability and reliability of capacitive devices [13, 14]. To avoid the electrostatic charging caused by external sources, custom-made packages with metal lids are used. To avoid the internal generation of electrostatic charging in the sensing element, screening electrodes are designed to surround entirely the active electrodes.

The inherent non-linearity associated with the asymmetry of the driving springs has raised additional stability concerns [15-17]. Consequently, great care has been taken to avoid any parametric, sub- or superharmonic resonances in the system.

## III. SENSOR MANUFACTURING

The manufacturing of the sensing element involves an innovative double-side processing and bonding of two capping composite wafers and a single-silicon substrate [9].

Fig. 5 illustrates the fabrication sequence that structures the top and bottom composite wafers. First, the pattern of the future glass inserts is defined by deep reactive ion etching (DRIE) in a single-crystal silicon wafer. Borosilicate glass is then reflowed in the created deep recesses [10, 11]. All the excess materials, silicon and glass, are removed by grinding and chemical-mechanical polishing (CMP). A contiguous layer of glass is kept on the outer surface of the composite wafers in order to enable the subsequent anodic bonding steps. The process continues by locally etching the glass inserts in those particular areas that are not intended for bonding, to form shallow recesses. A metal layer is deposited and patterned to form one part of the electrical press-contacts. An additional, distinct patterned metal layer is applied to one of the composite wafers to serve as getter for the various gases that may affect in long term the damping of the oscillations.

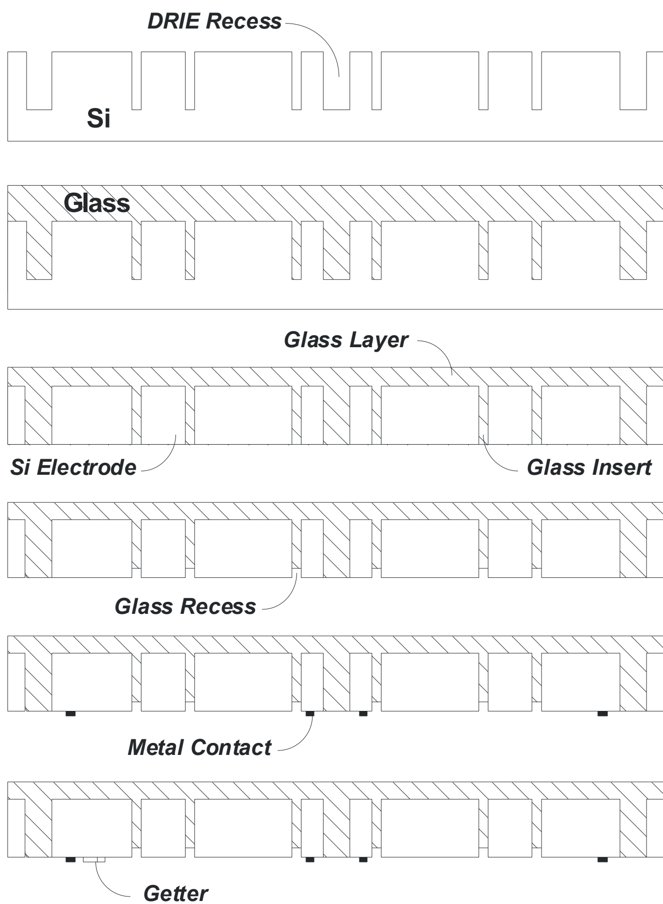


Figure 5. Processing sequence for structuring the composite capping wafers.

Note that, in order to achieve the required full symmetry, the corresponding elements of the top and bottom composite wafers have identical structure and geometry.

In order to achieve reliable thickness control, the MEMS elements are manufactured within the single-crystal silicon device layer of an SOI wafer.

Fig. 6 illustrates the fabrication sequence that structures the front surface of the SOI wafer. First, contact recesses are defined within the device layer to serve as requisite spacing for the top side electrical press-contacts. Then, electrode recesses are defined to serve as gaps for a number of subsequent top side capacitors. The combination of the contact and electrode recesses offers the possibility to create, at dedicated locations, silicon stoppers. An aluminium layer is deposited and patterned to form one part of the top side electrical press-contacts. Then, the upper-half profile of the beams is defined by DRIE.

Anodic bonding is used to permanently attach the machined SOI wafer and the top composite wafer to form the double-stack bonded wafer shown in Fig. 7.

Fig. 8 shows a detail of the formed double-stack bonded wafer, illustrating an example of top side capacitor, top side electrical press-contact and top side stopper.

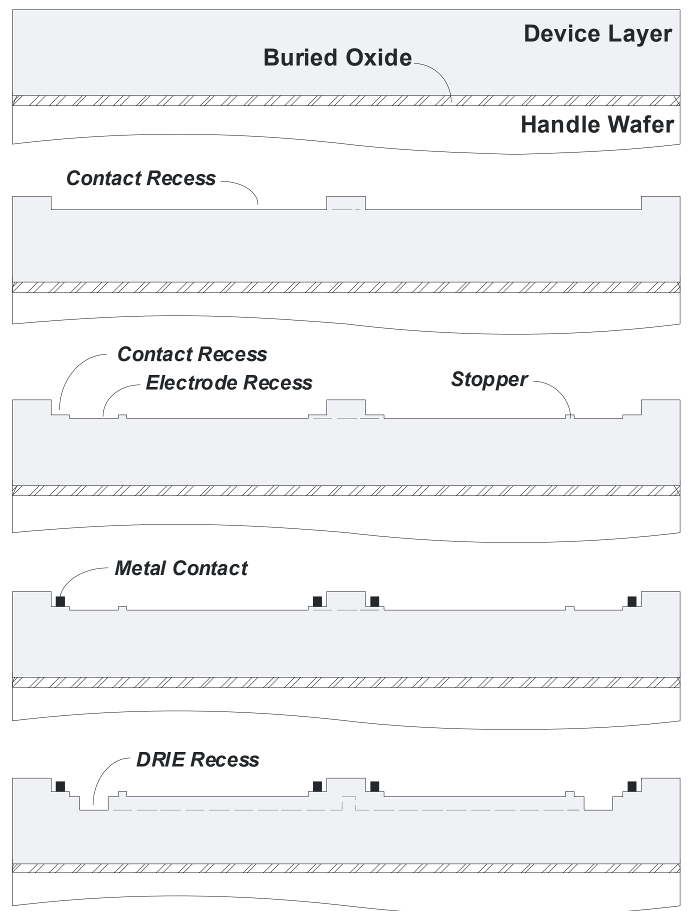


Figure 6. Processing sequence for structuring the front surface of the SOI wafer.

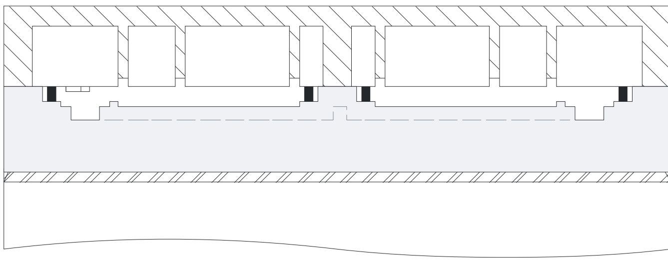

Figure 7. Double-stack bonded wafer.

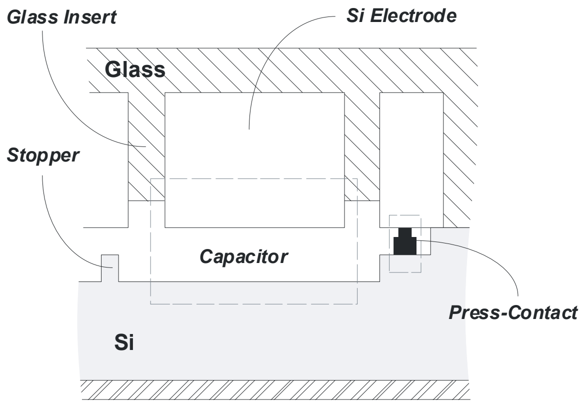


Figure 8. Detail of the double-stack bonded wafer.

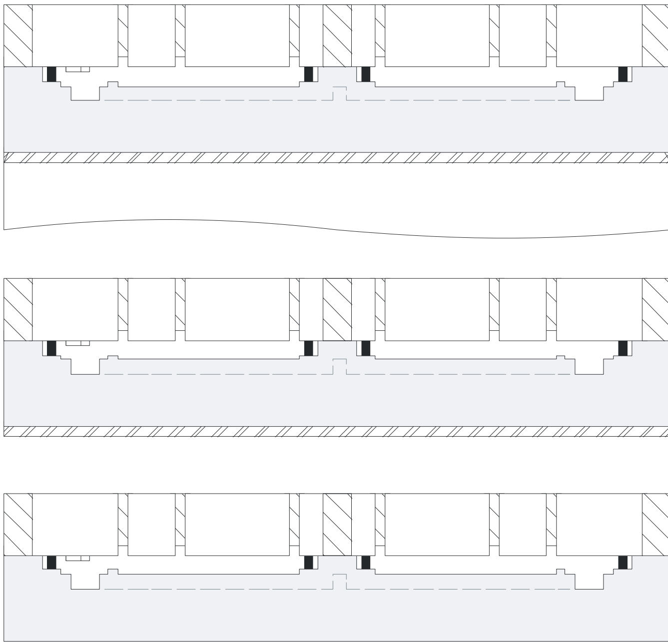

Figure 9. Thinning the double-stack bonded wafer.

Fig. 9 illustrates the fabrication sequence that removes the excess materials from the double-stack wafer. Grinding, followed by chemical-mechanical polishing (CMP), is used to remove the contiguous layer of glass, thus exposing the silicon pattern of the top composite wafer. Grinding, followed by reactive ion etching with etch stop on the buried oxide layer, is used to remove the handle wafer. Wet etching is then used to remove the buried oxide, thus exposing the back surface of the device layer.

Fig. 10 illustrates the fabrication sequence that structures the back surface of the double-stack bonded wafer. Identical processing sequence and layer geometry as on the front surface are used. The masses and the beams are formed and released in the process.

Anodic bonding, performed in high-vacuum, is used to permanently attach the machined double-stack wafer and the bottom composite wafer to form the triple-stack bonded wafer shown in Fig. 11. Bottom side press-contacts and capacitors, similar to those illustrated in Fig. 8, are formed in the process.

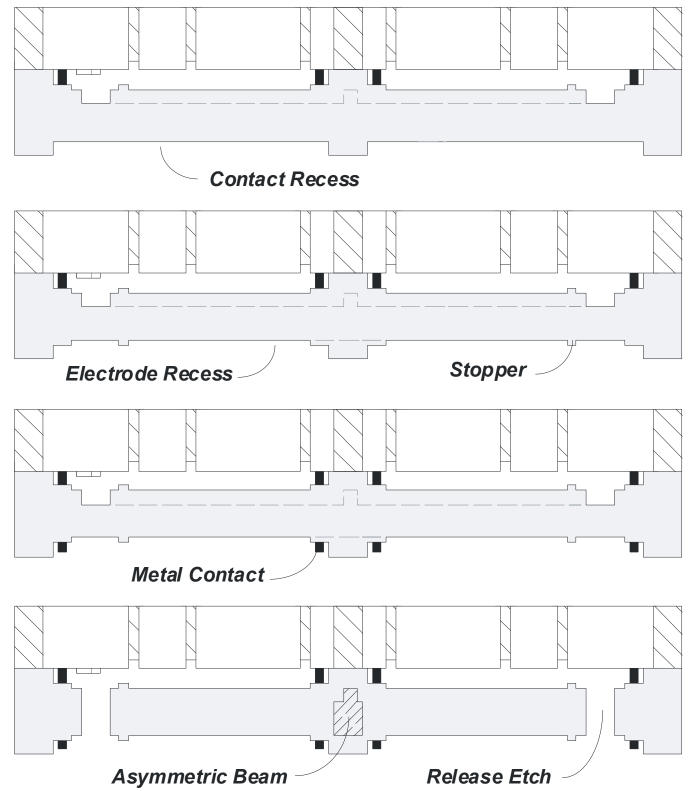


Figure 10. Processing sequence
for structuring the back surface of the double-stack wafer.

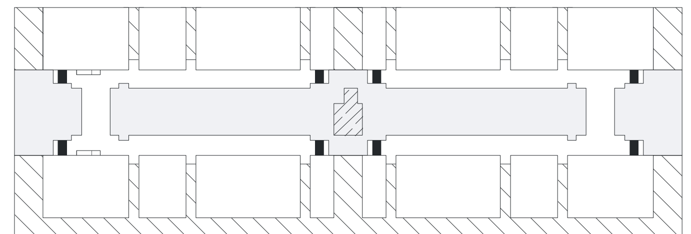

Figure 11. Triple-stack bonded wafer.

The anodic bonding between a silicon substrate and silicon-glass composite wafers allows the formation of a hermetic seal not only between the involved wafers, but between the internal silicon-glass interfaces of the composite wafers as well.

Fig. 12 illustrates the fabrication sequence that completes the structuring of the triple-stack bonded wafer. First, grinding, followed by CMP, is used to remove the contiguous glass layer, thus exposing the silicon pattern of the bottom composite wafer. Metal layers are then deposited and patterned on both surfaces of the triple-stack wafer to form the top and bottom pads. Finally, sawing is used to separate the wafer into dice.

Fig. 13 shows the top view of the sensing element, with the distinctive silicon-glass structure clearly visible.

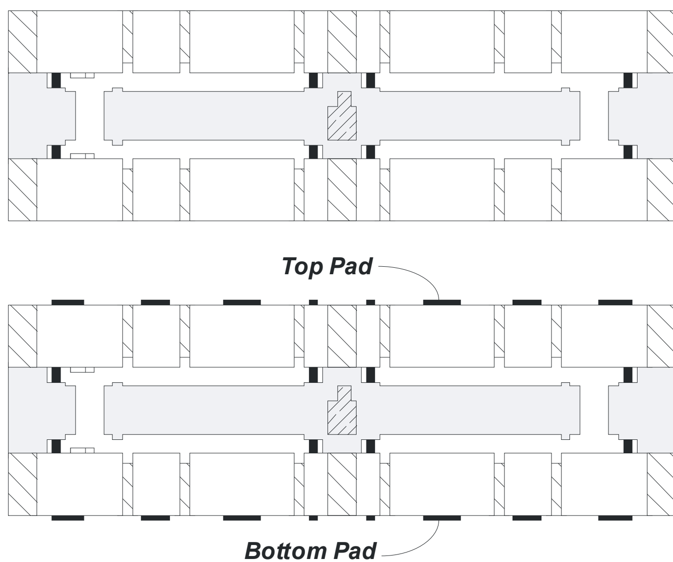


Figure 12. Processing sequence for structuring the triple-stack wafer.

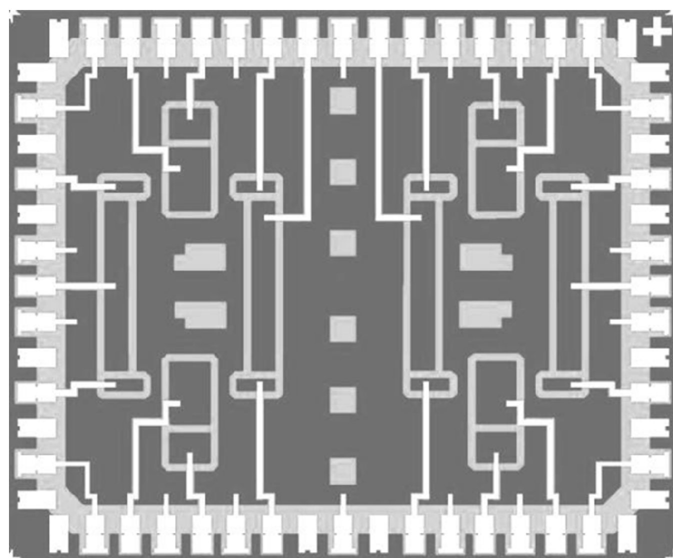

Figure 13. Top view of the sensing element.

## IV. SIGNAL PROCESSING

The signal processing in the SAR500 is based upon two main feedback loops, as shown in Fig. 14. The excitation loop is a positive feedback loop with automatic gain control (AGC), which keeps the drive mode of the sensor oscillating at its natural frequency, at constant amplitude. The detection loop has a negative feedback that reduces the Q factor of the sense mode to provide the required bandwidth of the gyroscope.

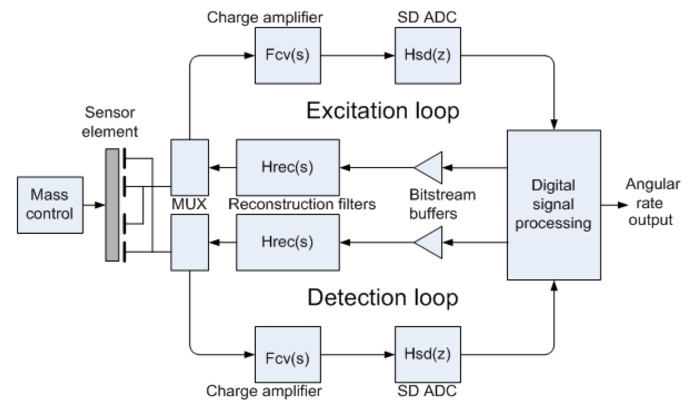


Figure 14. SAR500 system block diagram.

The capacitive sensor signal is read by a fully differential low-noise charge amplifier with correlated double sampling. A 5$^{th}$ order sigma-delta (SD) ADC converts the signal to a bit-stream for processing in the digital part of the feedback loop.

The digital signal processing provides a stable, high-resolution implementation of the loop filters and sigma-delta (SD) DACs for excitation and detection feedback. It also performs low-noise synchronous demodulation and compensates for temperature drift of bias and scale factor.

The analog reconstruction filter is matched to the SD DAC, as illustrated in Fig. 15, to remove the quantization noise from the analog voltage that is fed back to the sensing element.

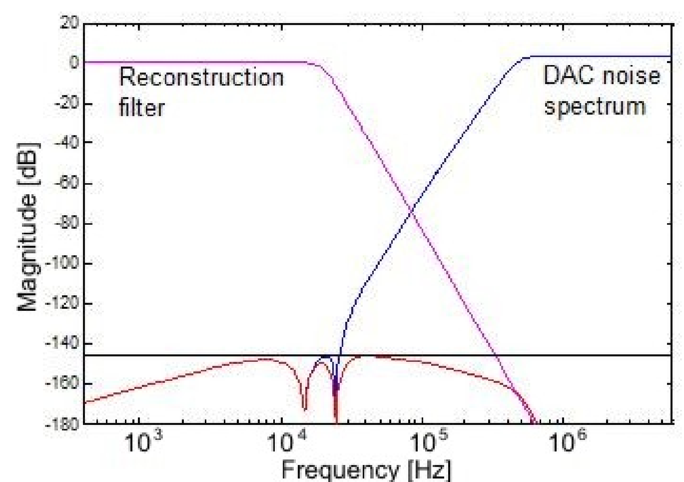


Figure 15. Matching of SD DAC and reconstruction filters.

Since the gyroscope operates in a narrow bandwidth close to 10 kHz, the 1/f noise is not a major issue in most of the circuits. Yet some of the circuits depend on the stability of the reference voltage and are therefore quite sensitive to the low frequency noise. Great care has been taken to reduce the impact of the 1/f noise in those particular circuits.

Though the analog chip contains a voltage reference, in order to achieve the targeted long-term stability, an external voltage reference is used.

The readout and force feedback in the two loops is time multiplexed at a frequency of about 300 kHz. Innovative algorithms are used to generate feedback signals for quadrature compensation and frequency matching.

The electronics is realized on two chips, an analog and a digital ASIC.

The read-out amplifiers, sigma-delta ADCs, reconstruction filters and voltage reference have been implemented in a 0.35 µm process with a 20V process option, as shown in Fig. 16.

The digital circuits are currently implemented in an FPGA, but will be realized in a 90 nm structured ASIC at a later stage. A 32 bit microcontroller is included to perform temperature compensation and other auxiliary tasks.

The gyroscope is configured as an SPI slave for efficient readout of angular rate and other data.

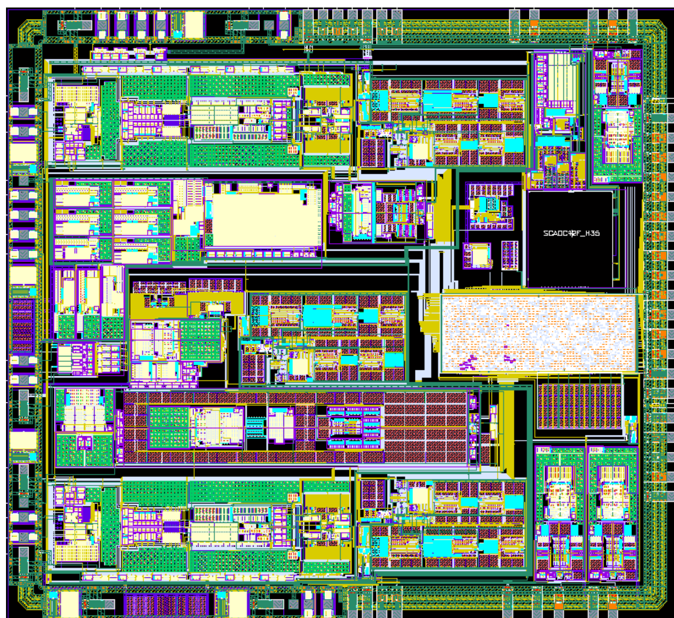

Figure 16. Layout of the analog ASIC.

## V. Assembly and Packaging

The packaging has a major influence on the performance of the device, especially with respect to factors such as long-term drift and stability.

Since the analog ASIC is a major heat source, capable of inducing significant temperature gradients across the sensing element, the sensing element and the analog ASIC are mounted in distinct, separated packages, subsequently soldered together.

The main design requirements for the SAR500 packages were: i) full symmetry around the sensing element (with respect to mechanical and thermal loads); ii) reduced levels of transmitted stress and strain to the sensing element; iii) high thermal efficiency (fast evacuation of heat from the analog ASIC and uniform temperature distribution inside the sensing element).

The sensing element is mounted in a fully symmetrical, custom-made 16 pin, side-brazed ceramic package, shown in Fig. 17. The high thermal efficiency of the package is achieved by using internally a large number of dedicated thermal vias and metal layers. Two identical, metal lids are subsequently attached in high vacuum on either sides of the package by electron-beam welding, thus sealing hermetically the sensing element. The size of the 16 pin package, including the pins, is 14.8 mm x 14.8 mm x 3.8 mm.

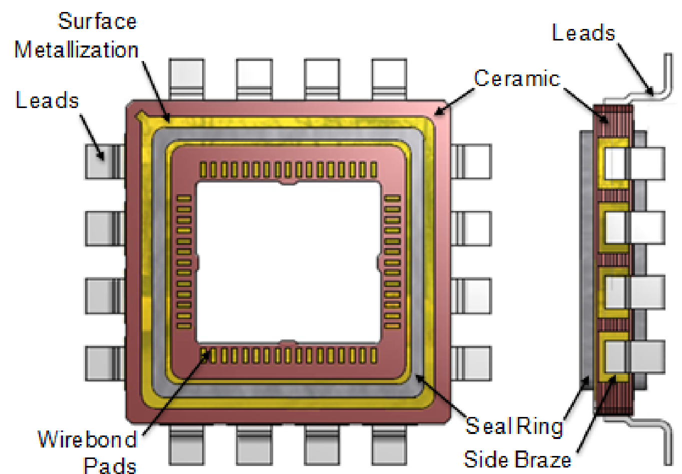


Figure 17. Top and side views of the 16 pin ceramic package.

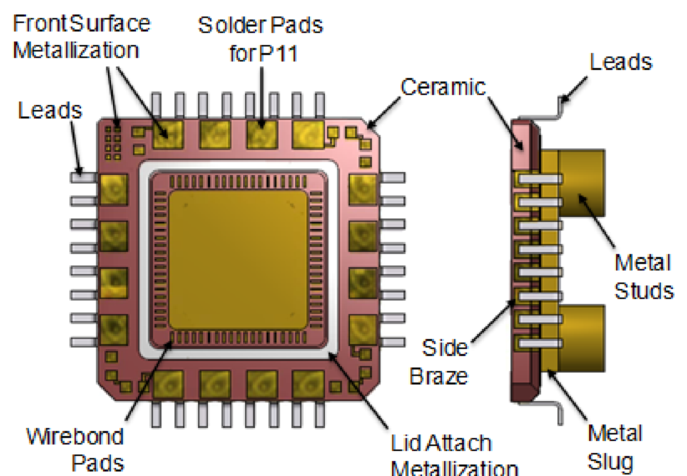


Figure 18. Top and side views of the 32 pin ceramic package.

The ASIC is mounted in a custom-made 32 pin, side-brazed ceramic package, shown in Fig. 18. The high thermal efficiency of the package is achieved by using a CuW thermal slug that is in direct physical contact with the ASIC. The thermal slug is provided with four filleted metal studs for versatile mounting on 'heat sinks'. A metal lid is subsequently soldered in inert atmosphere. The size of the 32 pin package, including the pins, is 17.6 mm x 17.6 mm x 5.0 mm.

Finally, the two ceramic packages are soldered on top of each other, as shown in Fig. 19.

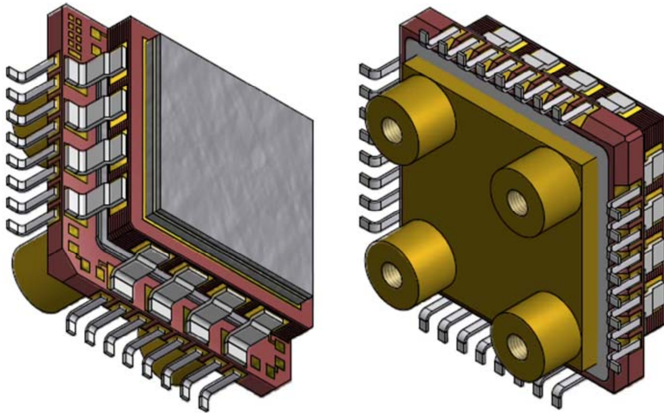

Figure 19. Bird-eye views of the assembled SAR500 packages.

## VI. CONCLUSIONS

SAR500, a novel high-precision, low-noise, high-stability, calibrated and compensated digital oscillatory gyroscope with north seeking capability, is reported.

The SAR500 contains a Butterfly™ MEMS die and an analog ASIC, individually housed in rigid, thermally efficient, custom-made ceramic packages. An FPGA or a digital ASIC contains the needed control and functional algorithms to achieve the superior performance. The gyroscope is configured as an SPI slave for efficient readout of angular rate.

The device is factory-calibrated and compensated for temperature effects to provide high-accuracy digital output over a broad temperature range. Optimized tuning of the excitation and detection frequencies, as well as optimized mechanical and electrical balancing of the dual masses result in low sensitivity to shock and vibrations.

By utilizing a newly developed sealed cavity technology, the vibrating masses of the sensing element are contained within the low-pressure hermetic environment needed for high Q factors.

The target performance elements of the device are: operation range = ±500 °/s, scale factor accuracy = ±300 ppm, angular random walk = 0.002 °/√h, in-run bias stability = 0.04 °/h and bias repeatability = 0.1 °/h.


## ACKNOWLEDGMENTS

The authors would like to thank Niels Hedenstierna (Imego AB) and Eskild Westby (West Consult AS) for their technical advice during the conceptual phase and sensor design.

Imego AB is specially acknowledged for their extensive contribution to the design of the associated electronic circuits.

The authors would also like to thank Plan Optik AG for their support in manufacturing and processing the composite wafers.


## REFERENCES


[1] "MEMS Accelerometer, Gyroscope and IMU market 2008-2013", Yole Développement, 2009.

[2] N. Hedenstierna, S. Habibi, S. M. Nilsen, T. Kvisterøy, and G. U. Jensen, "Bulk micromachined angular rate sensor based on the 'butterfly'-gyro structure," MEMS 2001, pp. 178–181, 2001.

[3] B. Chaumet, B. Leverrier, C. Rougeot, and S. Bouyat, "A new silicon tuning fork gyroscope for aerospace applications," Syposium Gyro Technology 2009, Karlsruhe, Sep. 2009.

[4] A. A. Trusov, A. R. Schofield, and A. M. Shkel, "Vacuum packaged silicon MEMS gyroscope with Q-factor above 0.5 million," IMAPS Device Packaging 2010, March 2010.

[5] G. Anderson, N. Hedenstierna, and P. Svensson, "An arrangement for measuring angular velocity," European Patent No. EP 1467179 A2, Autoliv Development AB, Oct. 2004.

[6] A. Blomqvist, "Oscillating micro-mechanical sensor of angular velocity," US Patent No. US 7325451 B2, VTI Technologies Oy, Feb. 2008.

[7] A. Blomqvist, "Oscillating micro-mechanical sensor of angular velocity," US Patent No. US 7454971 B2, VTI Technologies Oy, Nov. 2008.

[8] D. Lapadatu, T. Kvisterøy, and H. Jakobsen, "Micromechanical Device," US Patent No. US 6684699 B1, Sensonor asa, Feb. 2004.

[9] D. Lapadatu, G. Kittilsland, S. Jacobsen, "Method for manufacturing a hermetically sealed structure," Patent application, Sensonor Technologies AS, Apr. 2010.

[10] H.-J. Quentzer, A. V. Schultz, and P. Merz, "Glass-type planar substrate, use thereof, and method for the production thereof," International Patent No. WO 2004/030057 A1, Fraunhofer-Gesellschaft zur Förderung der angewandten Forschung e.V., Apr. 2004.

[11] H.-J. Quentzer, A. V. Schultz, B. Wagner, and P. Merz, "Method of structuring a flat substrate consisting of a glass-type material," US Patent No. US 2004/018051 A1, Fraunhofer-Gesellschaft zur Förderung der angewandten Forschung e.V., Sep. 2004.

[12] R. N. Candler, A. Duwel, M. Varghese, S. A. Chandorkar, M. A. Hopcroft, W.-T. Park, K. Bongsang, G. Yama, A. Partridge, M. Lutz, and T. W. Kenny, "Impact of geometry on thermoelastic dissipation in micromechanical resonant beams," JMEMS, Vol 15, No 4, pp. 927–934, Aug. 2006.

[13] A.-M. Kärkkäinen, "MEMS based voltage references," VTT Publications 613, 2006.

[14] J. Wibbeler, G. Pfeifer, and M. Hietschold, "Parasitic charging of dielectric surfaces in capacitive microelectromechanical systems (MEMS)," Sensors and Actuators A, Vol. 71, pp. 74–80, 1998.

[15] A. H Nayfeh and M. I. Younis, "Dynamics of MEMS resonators under superharmonic and subharmonic excitations," J. Micromech. Microeng., Vol. 15, pp. 1840–1847, 2005.

[16] L. A. Oropeza-Ramos and K. L. Turner, "Parametric Resonance Amplification in a MEMGyroscope," IEEE Sensors 2005., Nov. 2005.

[17] B. J. Gallacher, J. S. Burdess, and K. M. Harish, "A control scheme for a MEMS electrostatic resonant gyroscope excited using combined parametric excitation and harmonic forcing," J. Micromech. Microeng., Vol. 16, pp. 320–331, 2006.